PHYSICAL REVIEW B VOLUME 18, NUMBER 6 15 SEPTEMBER 1978

Chemical reactions and local charge redistribution at metal-CdS and CdSe interfaces

L. J. Brillson
Xerox Webster Research Center, Webster, New York 14580
(Received 21 October 1977)

The surface electronic structure of CdS and CdSe has been studied during the initial stages of Schottky-barrier formation with metals. Surface photovoltage spectroscopy, low-energy-electron-loss spectroscopy, and ultraviolet photoemission measurements taken as a function of metal overlayer coverage show that interface chemical reactions and local charge redistribution dominate the Schottky-barrier formation for both of these semiconductors. Despite the reported contrast in Fermi-level pinning behavior of CdS and CdSe, intrinsic surface states play no role in determining their Schottky-barrier heights. The microscopic metal-semiconductor bonding causes work-function and band-bending changes which determine the macroscopic space-charge characteristics of the interface. A critical heat of reaction $\Delta H_R^C \sim 0.5$ eV/(metal atom) characterizes the compound formation inferred from alterations in the interface dielectric properties.

I. INTRODUCTION

Recent studies of metal-semiconductor contacts have focused on the local bonding at the interface. Several groups have reported electronic features produced by metals on clean semiconductor surfaces which may affect the ultimate Schottky-barrier properties.[1-13] Perhaps the most representative of these semiconductors are CdS and CdSe, which exhibit interface behavior midway between those of covalent and ionic semiconductors. Furthermore, differences in interface behavior of CdS and CdSe have until now been attributed[14] to variations in intrinsic surface-state densities.[15] In this paper, I present results for CdS and CdSe during the initial Schottky-barrier formation with various metals. A general set of metal-induced phenomena are observed for both reactive and unreactive metals. These results show that intrinsic surface states do not determine the barrier heights of these metal-semiconductor contacts. Rather, metals induce microscopic charge redistribution of the interfaces which do account for these barriers. For reactive metals, these contacts are dominated by interface compounds that are formed. For unreactive metals, the barrier formation is related to discrete metal-induced surface states. Bulk heats of formation and reaction of the interface constituents are used to characterize these two regimes. Furthermore, the extrinsic phenomena measured for CdS and CdSe can be shown to apply to a wide variety of semiconductors, particularly those with covalent bonding.

CdS and CdSe can be viewed as representative semiconductors because they span a wide range of interface behavior with metals. This is illustrated in Fig. 1. The index of interface behavior[14,16,17] S is plotted versus the heat of compound formation[18] ΔH_F for a variety of semiconductors. The parameter S is defined by

$$qV_B = S(\phi_M - \chi_{SC}) + C \ , \tag{1}$$

where qV_B is the band bending in the surface-space-charge region of the semiconductor, ϕ_M and χ_{SC} are the work function and electron affinity of metal and semiconductor, respectively, and C is a constant. These parameters are illustrated schematically in the insert of Fig. 1. Electronic structure changes have been studied elsewhere for metals on the covalent semiconductors Si,[1-5] Ge,[3] GaAs,[3,6,7] GaSb,[7-9] InAs,[7] InP,[10,11] and GaP.[7] However, Fig. 1 shows that the more ionic semiconductors CdS and CdSe span an even wider range of interface behavior and may therefore be expected to exhibit more general interface phenomena. It is noteworthy that the curve fit to the data points is virtually identical to the well-known curve of interface behavior S versus electronegativity difference ΔX of the same semiconductor constituents.[16] While ΔX and ΔH_F can be related via linear[19] or quadratic[20] expressions, Fig. 1 emphasizes the direct relationship between chemical reactivity of the interface and Schottky-barrier phenomena. This curve shows that covalent semiconductors have lower heats of formation and thus are less stable than ionic semiconductors against chemical reaction with metals. As will be shown, a critical heat of reaction exists for metals on CdS and CdSe, below which interface compound formation is detected. Because CdS and CdSe possess intermediate heats of formation, such a critical heat of reaction will apply to semiconductors of both intermediate as well as covalent bonding.

A complementary set of highly surface-sensitive UHV spectroscopies were used to study the intimate metal-semiconductor contacts. Low energy

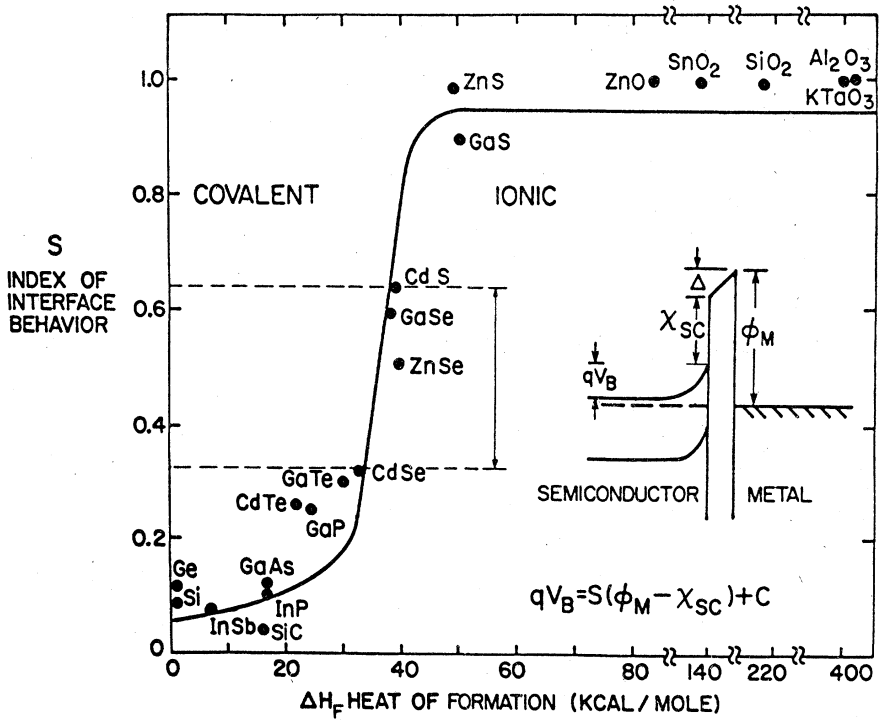

FIG. 1. The index of interface behavior S plotted vs heat of compound formation ΔH_F. S values taken from Ref. 14.

(100 eV) electron-loss spectroscopy (ELS) was employed to monitor changes in electronic excitations caused by interface chemical reactions. Because the escape depth of these electrons is ≤ 5 Å,[21,22] the chemical effects can be probed with a resolution of monolayer thickness. The surface photovoltage spectroscopy (SPS) technique measured both metal-induced surface states as well as the variations in band bending and work function associated with increasing metal coverage. SPS is also highly surface-sensitive, exhibiting pronounced features corresponding to submonolayer adsorption on semiconductors.[23,24] Ultraviolet photoemission spectroscopy (UPS) provided a complementary measurement of the surface work function and uniquely determined the Fermi level with respect to the band edges. Again, the escape-depth resolution provided sensitivity to only the top few monolayers. From this combination of techniques, changes in band bending with the surface space-charge region of the semiconductor could be distinguished from formation of dipoles at the intimate metal-semiconductor contact. Furthermore, the highly localized dipole formation and interface compound formation measured by this combination of techniques could be related to the ultimate Fermi-level position and barrier height of the junction.

The ultrahigh-vacuum (UHV) techniques employed to characterize the metal-semiconductor interfaces are described in Sec. II. ELS results are presented in Sec. III A which establish a critical heat of reaction for interface compound formation. Metal-induced surface states for unreactive metals are reported in Sec. III B, while dipole formation measurements are described in Sec. III C for both unreactive and reactive metals. Section III D deals with UPS measurements of dipole formation and Fermi-level stabilization. We discuss the influence of interfacial chemical reactions and microscopic dipole formation on the macroscopic interface properties for these and other semiconductors in Sec. IV. Finally, these results are summarized in Sec. V.

II. EXPERIMENTAL TECHNIQUES

The metal-semiconductor interfaces were prepared and characterized in a stainless steel UHV chamber with a base pressure $p \sim 6\times10^{-11}$ Torr. The CdS and CdSe specimens were "ultrahigh-purity" single crystals supplied by Eagle-Picher Ind. and Cleveland Crystals, Inc. with n-type carrier concentrations of $(1-4)\times10^{16}$ cm^{-3} (1-Ω cm resistivity). A single "intrinsic" CdS crystal (10^9-Ω cm resistivity) was also studied. These crystals were $4\times4\times15$ mm^3 bars with either $(10\bar{1}0)$ or $(11\bar{2}0)$ square faces. The bars were scribed with a diamond saw and cleaved in UHV with a tungsten carbide blade and an annealed Cu anvil.

The metals Al, Ag, Cu, and Au were evaporated from a W wire in a horizontal sidearm which could

be isolated from the main chamber by a metal straight-through valve. An air lock attached to this sidearm permitted evaporants to be changed without breaking vacuum. A quartz crystal and frequency counter monitored the metal deposition with a precision of 0.05–0.2 Å. Metal was evaporated at a rate 1–3 Å/min. with UHV chamber pressure rising to $2-5\times10^{-10}$ Torr. The evaporant was in the form of a collimated beam, into and out of which the cleaved crystal faces were rotated to obtain well-defined metal deposits. Surface-metal coverage and ambient contamination were monitored independently by Auger electron spectroscopy (AES) and x-ray photoelectron spectroscopy (XPS). These showed no detectable contamination (<1% monolayer equivalent) over the course of each experiment. In addition, LEED pattern measurements monitored the changes in surface atomic order with increasing metal coverage.

The SPS technique used to measure surface work function and band bending has been described elsewhere.[24,25] Briefly, it consists of monitoring the contact potential difference (CPD) between a vibrating Au reference probe and the semiconductor surface as a function of incident photon energy $h\nu$ from an ir-uv prism monochromator. This CPD could be measured continuously with a lock-in amplifier operating in a negative feedback circuit. The changes in slope $\Delta V_{CPD}/\Delta h\nu$ correspond to transitions to or from states within the band gap. Work-function changes associated with the band flattening under high-intensity, ($>10^{18}$ photons/cm^2), above band-gap illumination gave a measure of the band bending within the surface space-charge region.

ELS measurements consisted of electron beam excitation from a glancing incidence (~20°) electron gun and energy analysis of the backscattered electrons with a double-pass cylindrical mirror analyzer (CMA). Electron beam currents were typically 1 μA/cm^2 at 100-eV) incident energy. Second derivative spectra d^2N/dE^2 with a modulation voltage 0.5 V peak to peak yielded energy loss features with an overall resolution of 0.7 eV.

A hydrogen discharge lamp and vacuum-uv monochromator produced 10.2-eV radiation for UPS measurements. The uv light was directed to the specimen along the CMA and normal to the semiconductor surface by means of an elliptical mirror inside the CMA.[26] The surface sensitivity associated with 10.2-eV incident photon energy[22] proved ideal for this study since composite energy distribution curves (EDC's) could be obtained from both the thin metal overlayer and the underlying semiconductor. Multiple spectra of UPS, ELS, and SPS were averaged and processed with a Tracor Northern signal averager and Nova 2/10 minicomputer.

III. RESULTS

The metal-semiconductor interfaces to be discussed in this paper are: Al on (11$\bar{2}$0) CdSe and CdS, Cu on (11$\bar{2}$0) CdS, (10$\bar{1}$0) CdS, and (11$\bar{2}$0) CdSe, Ag on (10$\bar{1}$0) CdS and (11$\bar{2}$0) CdSe, and Au on (10$\bar{1}$0) CdS, (11$\bar{2}$0) CdS, and (11$\bar{2}$0) CdSe. This set of junctions permitted comparison of interface behavior between CdS and CdSe, between (10$\bar{1}$0) and (11$\bar{2}$0) semiconductor surfaces, and among metals of different interface reactivity.

A. Electron loss spectra of reactive vs unreactive interfaces

ELS spectra recorded as a function of metal overlayer coverage exhibited features belonging to two classes of chemical reactivity. Reactive metals on CdS and CdSe exhibited strong changes in ELS features which did not correspond to bulk-loss features of either semiconductor or metal. In contrast, unreactive metals showed only a simple superposition of metal and semiconductor loss features. As an example of a reactive interface, Fig. 2 shows ELS spectra for Al on (11$\bar{2}$0)

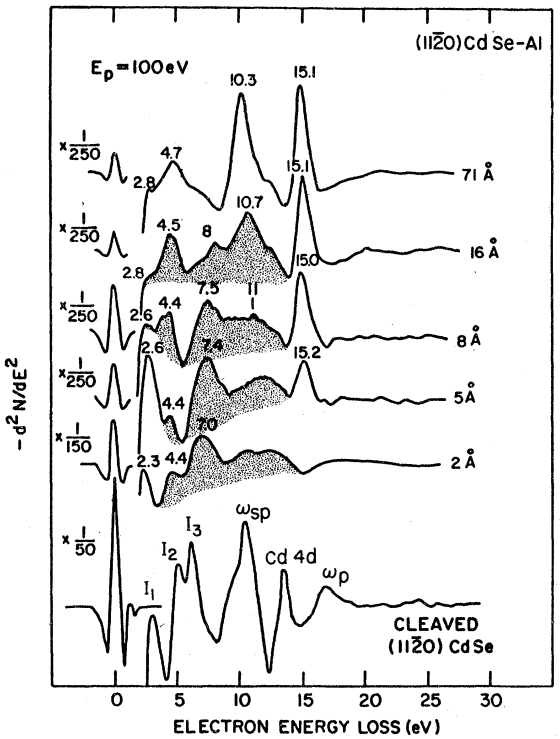

FIG. 2. ELS spectra of Al on cleaved (11$\bar{2}$0) CdSe as a function of metal overlayer coverage. Shaded regions correspond to features unrelated to bulk Al or CdSe.

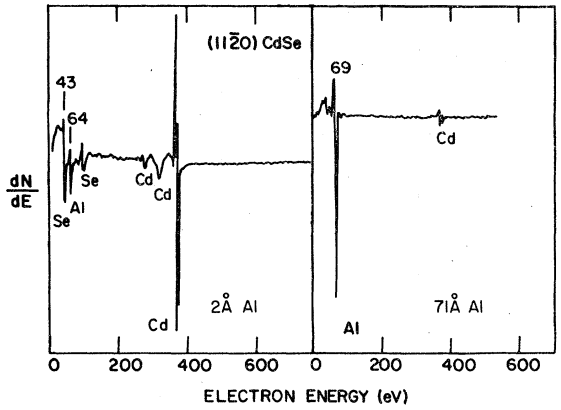

FIG. 3. AES spectra of 2 and 71-Å thick Al overlayers on (11$\bar{2}$0) CdSe. Incident electron beam energy was 2 kV.

CdSe as a function of metal overlayer thickness.[13] The cleaved CdSe surface exhibited peak features corresponding to bulk and surface plasmons, a core level transition from the Cd 4*d* level to the conduction band, as well as interband transitions.[27] These are labeled ω_{sp}, ω_p, Cd 4*d*, and I_1, I_2, I_3, respectively, in Fig. 2. With the initial deposition of 2 Å of Al, this ELS spectrum changes completely. Furthermore, the LEED pattern of the ordered CdSe surface disappears. Al reacts with the CdSe surface and produces a chemical shift of the *LMM* Al Auger peak for the metal overlayer on CdSe relative to the thick Al film. This chemical shift of 64 eV for the 2-Å surface layer to 69 eV for a 71-Å bulk film is shown in Fig. 3. The appearance of only one shifted Al *LMM* peak in the 2-Å AES spectrum is evidence that Al forms a thin, continuous film on CdSe rather than forming islands. If islands of bulk metal were produced, both shifted and unshifted *LMM* features would appear. The absence of any residual CdSe features in the 2-Å ELS spectrum of Fig. 2 is further evidence for a continuous Al overlayer.

At intermediate metal overlayer coverages, a new set of ELS features appear which ultimately become the surface and bulk plasmons of Al. These new features are indicated by the shading in Fig. 2. There is no superposition of CdSe and Al peak features. These features in fact arise from coupled interface plasmon modes which can be fitted to a four-layer interface model (e.g., semiconductor, reacted layer, metal, and vacuum) to obtain the dielectric constant of the reacted interface layer.[13] For Al on CdS and CdSe, these dielectric constants are lower and more ionic than those of the semiconductor substrates, consistent with the formation of Al chalcogenides.

Figure 4 illustrates ELS spectra for Cu on a cleaved CdS (10$\bar{1}$0) face. Analogous to the Al spectra, Cu on CdS removes the Cd 4*d* and surface plasmon peaks as well as the ordered CdS LEED pattern at monolayer coverages. Furthermore, electron loss spectra taken with a 200-eV incident-beam energy exhibit chemically-shifted *MMM* Auger features[28] at these coverages. Figure 5 shows such a chemically shifted feature at 61.2 eV as well as a second, unshifted *MMM* feature at 2–3 eV higher energy which appears at thicker overlayers. The observation of both shifted and unshifted Auger peak features is an indication of at least some island formation. However, normalized AES spectra[29] of the first several Cu monolayers yielded metal surface coverages consistent with deposition monitor thicknesses. The ELS spectra of Fig. 4 show that a new set of hybrid features unlike those of either metal or semiconductor appear at intermediate metal coverages. These peak features ultimately merge with the bulk excitations of Cu at thick overlayer coverages.[30,31]

In contrast to the ELS features of Cu on CdS, Ag deposited on a CdS (10$\bar{1}$0) face cleaved from the same crystal exhibited only a superposition of metal and semiconductor features. As shown in Fig. 6, the ELS feature of CdS, particularly the Cd 4*d* level transition at 13.5 eV and the surface plasmon at 10.5 eV, decrease gradually with increasing coverage and are slowly dominated by the excitation features of bulk Ag.[31,32] The ordered CdS LEED display persists for coverages of several monolayers but shows no changes in the spot pattern. Normalized XPS (Refs. 33 and 34) and AES spectra showed incomplete Ag coverage of CdS up to equivalent deposition thicknesses of several monolayers. This behavior indicates possible island formation, which is more likely to occur for such less reactive interface bonding.[35] There is no evidence for substantial diffusion of Ag into the CdS since the ordered LEED pattern is not disrupted by the initial Ag deposition, in contrast to LEED pattern changes observed with metal diffusion into Si.[2] Furthermore, Ag exhibits negligible bulk diffusion in CdS,[36] and CdSe,[37] near room temperature.

The ELS spectra of Au on (11$\bar{2}$0) CdSe shown in Fig. 7 exhibit features whose behavior with increasing overlayer coverage is similar to that of the Ag-CdS interface. The ELS peak features of the CdSe appear only slightly altered with increasing Au deposition. Again the ordered CdSe LEED pattern persists for several equivalent monolayer thicknesses of Au without any significant changes in the spot pattern. Both XPS and AES measurements indicated less than complete metal surface coverage of the semiconductor even for an equivalent thickness of 74 Å. Again these features suggested island formation, consistent with a rela-

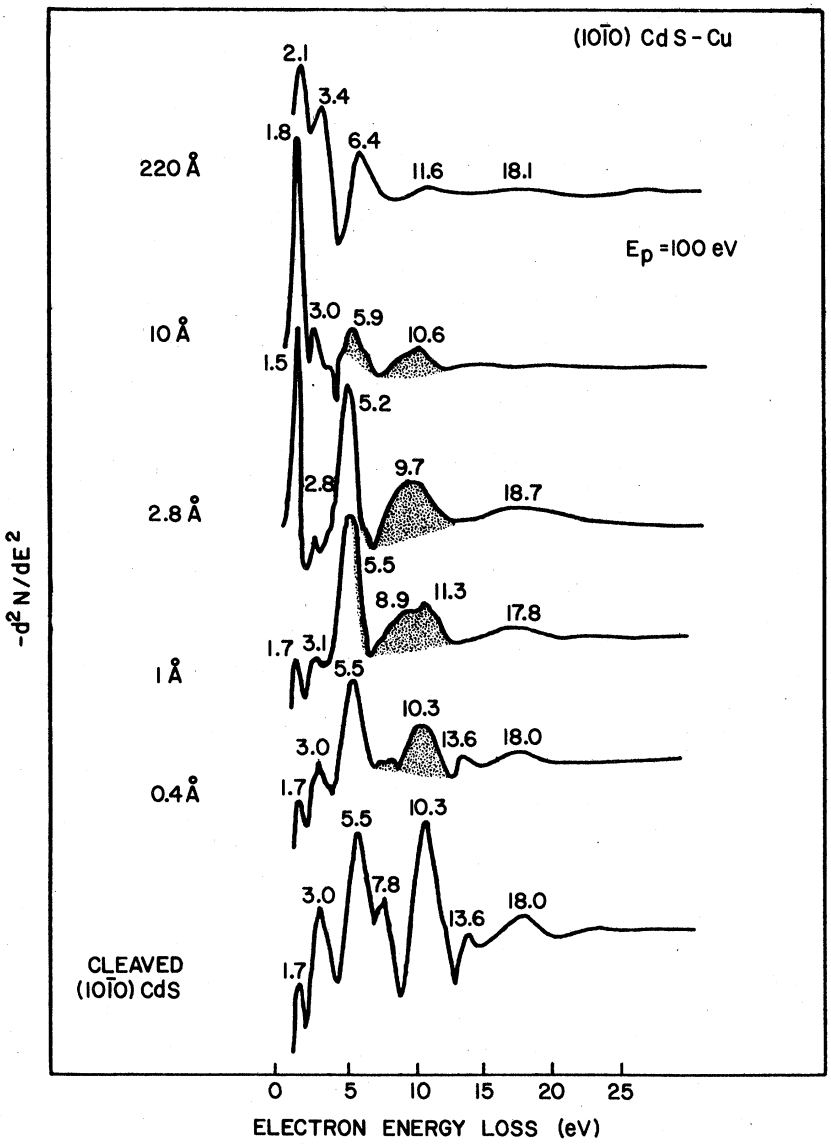

FIG. 4. ELS spectra of Cu on cleaved (10$\bar{1}$0) CdS as a function of metal overlayer coverage. Shaded regions correspond to features unrelated to bulk Cu or CdS.

tively weak metal-semiconductor bonding. Diffusion of Au into CdS near room temperature is also negligible.[36]

Because the plasmon and interband transitions of Cu, Ag, and Au are more complex than those of Al,[38] and because of variations in thickness due to possible island formation, it was difficult to gauge the coupled-mode behavior at the Cu-, Ag-, Au-semiconductor interfaces. Nevertheless, the qualitative difference in ELS spectra between reactive metals such as Al and Cu and unreactive metals such as Ag and Au on CdS and CdSe establishes a critical heat of reactivity for metals with these semiconductors. This critical heat of reactivity is described in Sec. V for CdS and CdSe as well as more covalently bonded semiconductors.

B. Metal-induced surface states

While reactive metals can form surface compounds with new electronic properties, unreactive metals can also produce effects on surface electronic structure. In particular, Au on cleaved CdS and CdSe induces discrete new states located at energies within the semiconductor band gaps. These new interface states are particularly significant in view of the complete absence of any intrinsic surface states on cleaved (11$\bar{2}$0) or (10$\bar{1}$0) CdS and CdSe.[25,26] Figure 8 shows SPS curves measured as a function of metal overlayer coverage for Au on cleaved (10$\bar{1}$0) CdS. The cleaved CdS features correspond to band-to-band transitions at the absorption edge as well as bulk-trap

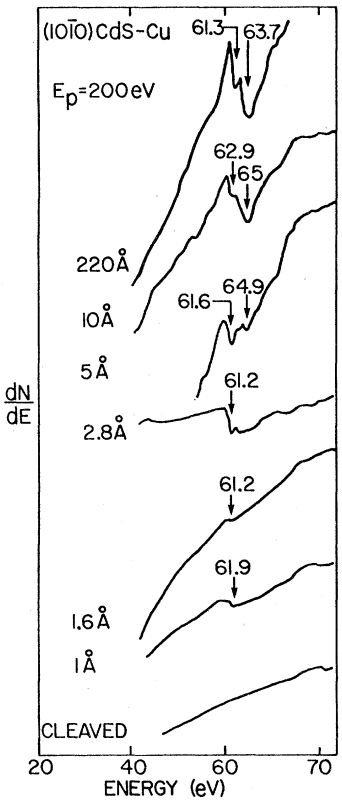

FIG. 5. ELS spectra displaying Cu *MMM* Auger losses as a function of metal overlayer coverage.

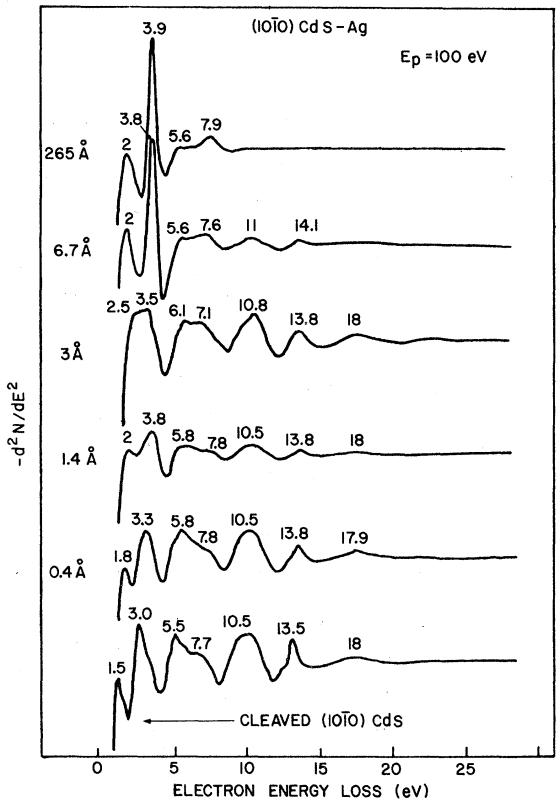

FIG. 6. ELS spectra of Ag on cleaved (10$\bar{1}$0) CdS as a function of metal overlayer thickness. The same CdS crystal was studied in Fig. 4.

transitions reported elsewhere.[39] These bulk features appear in all CdS SPS curves. With initial Au deposition, new SPS features appear which correspond to transitions to new states located 1.75 eV above the valence band and from states located 1 eV below the conduction-band edge. These transitions are illustrated in Fig. 9(a) along with the change in surface work function measured by SPS. It should be noted that these new electronic features appear for a relatively low equivalent monolayer coverage $\theta = 0.11$ of Au. With increasing coverage, the 1.0-eV transition disappears and the SPS spectra display features corresponding to complementary transitions into the state 1.75 eV above the valence-band edge and out of this state to the conduction-band edge 0.75 eV above. This is illustrated in Fig. 9(b). This band-gap state shifts in energy with increasing coverage [Fig. 9(c)], then is obscured by the thickening metal overlayer.

Extrinsic states also appear for Au on intrinsic (10^9 Ω cm) CdS at approximately the same energies. For comparable overlayer coverages, the positions of these states increase from 1.76 to 1.86 eV above the valence band with increasing coverages. Since the Fermi-level of 10^9-Ω cm CdS lies 0.53 eV further away from the conduction band than that of 1-Ω cm CdS, these SPS results show that bulk Fermi-level positions of CdS do not affect the interface state behavior of the metal-semiconductor contact.

The new SPS features induced by Au overlayers are not associated with trap levels of Au diffused into CdS, which have been observed by photoluminescence techniques.[40] As already mentioned, Au exhibits negligible bulk diffusion in CdS at temperatures $T \lesssim 300°$ C.[36] Furthermore, Au produced the new SPS features in the absence of any thick metal reservoir or any incident electron beam, both of which could have provided a driving force for bulk diffusion. Figure 9 also shows that the movement of the metal-induced state from 1.75 to 1.83 eV above the valence band with increasing overlayer thickness is opposite in direction to the Fermi level, which moves toward the valence band and the surface work function increases. Because of the sharpness of the SPS features at 1.75 and 0.75 eV in Fig. 8, this band-

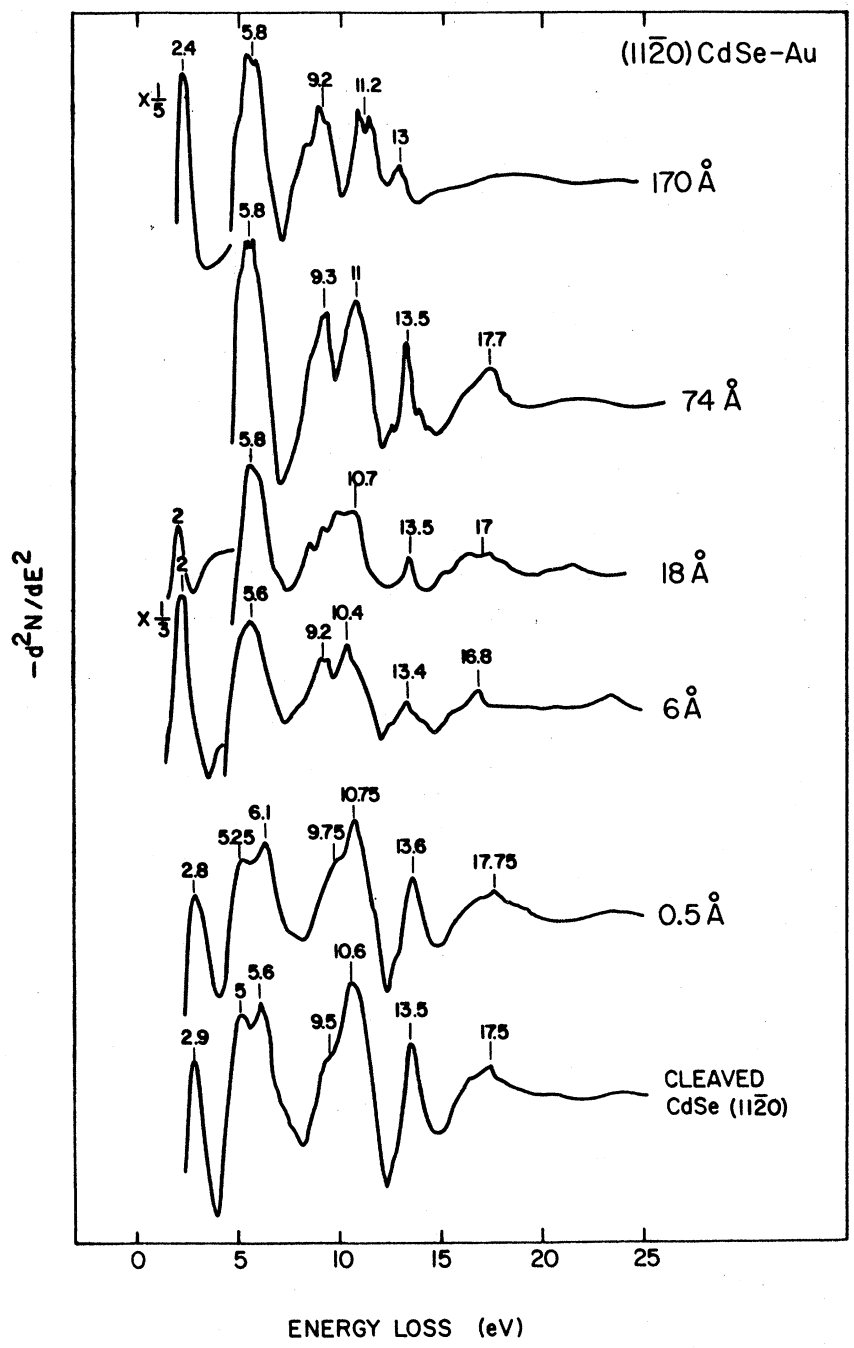

FIG. 7. ELS spectra of Au on cleaved (11$\bar{2}$0) CdSe as a function of metal overlayer thickness. The Au thickness values correspond to equivalent overlayer thicknesses.

gap feature is considered to be a discrete level rather than a broad continuum of states. Thus Au on CdS forms discrete chemisorption levels in the band gap before the Fermi level stabilizes and thus before the adsorbed Au exhibits metallic behavior.

Submonolayer coverages of Au on (11$\bar{2}$0) CdSe also induce new states in the semiconductor band gap. Figure 10 shows SPS spectra of Au on cleaved (11$\bar{2}$0) CdSe for different metal overlayer coverages. Analogous to CdS, the cleaved CdSe surface exhibits features corresponding to band-to-band transitions at the band edge as well as a bulk-trap transition determined previously.[26] With initial metal deposition, new SPS features appear which correspond to a 1.26-eV transition from a band-gap level to the conduction-band edge and a 1.14-eV transition from the valence band into a

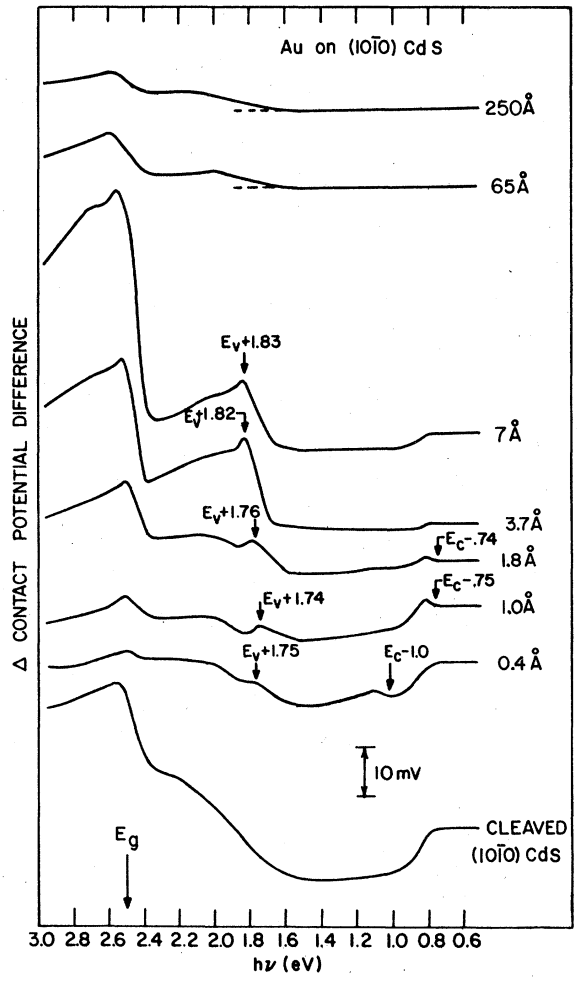

FIG. 8. SPS spectra of Au on cleaved (10$\bar{1}$0) CdS as a function of equivalent metal overlayer thickness. Arrows indicate transitions to and from metal-induced states within the band gap of energy E_g.

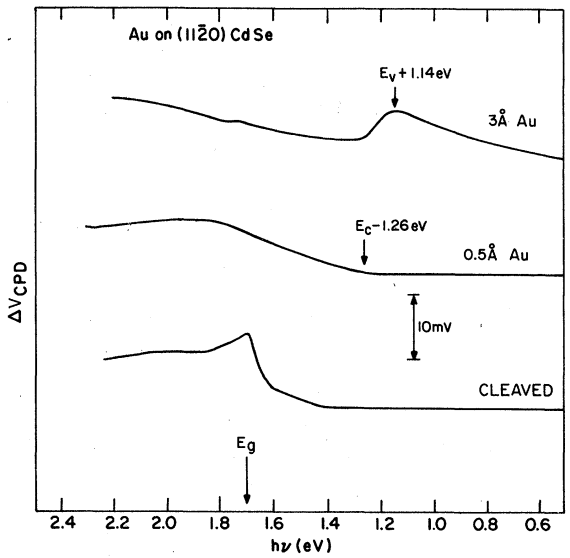

FIG. 10. SPS spectra of Au on cleaved (11$\bar{2}$0) CdSe for different metal overlayer thicknesses. Arrows indicate transitions to and from states within the band gap for energy E_g.

second level. Those levels are unrelated to any bulk dopant levels of Au in CdSe.[40]

Initial deposition of Ag and Cu on CdS also produced new levels at 1.96 and 1.8 eV respectively above the valence-band edge. However, these features could not be monitored for higher metal coverage because of significantly lower photovoltage response.

The Au-induced states which persist with increased overlayer coverage lie at energies in the band gap which are close to the ultimate Fermi-level positions of the macroscopic metal-semiconductor contact. Mead and Spitzer have determined

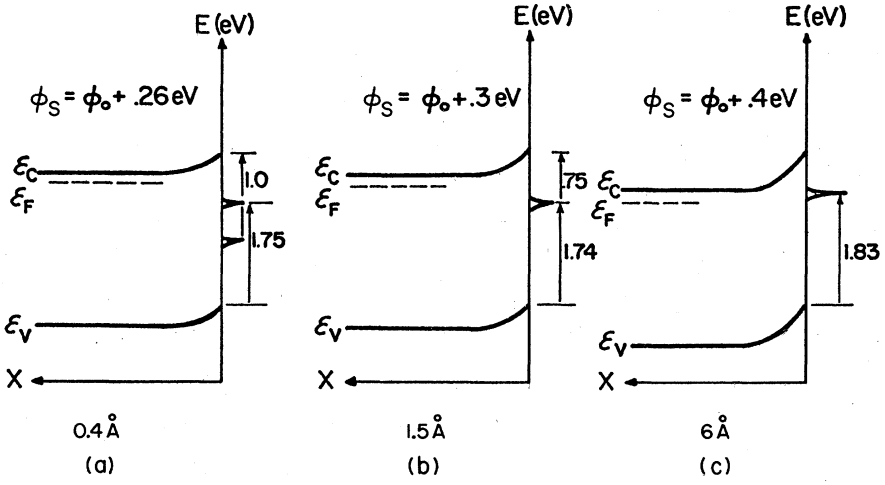

FIG. 9. Schematic energy-level diagram of optical transitions in the band gap of CdS corresponding to the SPS features of Fig. 8. ϕ_s is the work function of each surface.

TABLE I. Energy level positions above valence band E_V of Au-induced states and macroscopic Fermi levels of Au-CdS and CdSe interfaces. Barrier heights obtained from Ref. 41.

Interface	Barrier height (eV)	Macroscopic Fermi level position above E_v (eV)	Metal-induced level position above E_v (eV)
Au-CdS	0.8	1.65	1.75 [a]
			1.50
Au-CdSe	0.5	1.25	1.14 [a]
			0.45

[a] Persists at higher metal coverage.

the barrier heights of Au on CdS and CdSe by internal photoemission.[41] The Fermi-level positions derived from these barrier heights are given in Table I along with the energy level positions of the extrinsic states measured by SPS. As shown, the levels observed to persist with increased metal coverage are in good agreement with the ultimate Fermi-level positions of the respective contacts. Coupled with the absence of any intrinsic surface states or chemical reactions, this correspondence establishes the metal-induced surface states as the only measured features which can influence the Schottky-barrier formation.

C. Dipole formation of reactive and unreactive interfaces

The presence of new extrinsic surface states or chemical reaction at metal-semiconductor contacts causes a local charge redistribution and the formation of interface dipoles. Until now, the dipole formation commonly inferred from macroscopic interface experiments has been attributed to intrinsic surface states of the semiconductor,[42] which are not present on CdS and CdSe.[25,26] Here, interface dipoles were measured from the effective change in semiconductor electron affinity χ during the initial stages of Schottky-barrier formation of Au, Ag, and Cu on $(10\bar{1}0)$ CdS and Au on $(11\bar{2}0)$ CdSe.

The changes in electron affinity $\Delta\chi$ were determined from the relation

$$\Delta\chi = \Delta\phi - \Delta qV_B , \qquad (1)$$

where $\Delta\phi$ is the change in surface work function measured by SPS and ΔqV_B is the change in band bending determined from the band flattening under intense, band-gap illumination. These parameters are illustrated schematically in the insert of Fig. 1. The measured values of $\Delta\phi$ and ΔqV_B represent averages taken from several areas of the same crystal surface. Standard deviations were <0.1 eV for $\Delta\phi$ and <0.01 eV for ΔqV_B.

Figure 11 displays the changes in $\Delta\phi$ and ΔqV_B for Au on cleaved $(10\bar{1}0)$ CdS. With initial Au deposition, $\Delta\phi$ increases, whereas ΔqV_B remains constant or decreases slightly. With increasing metal deposition, both $\Delta\phi$ and ΔqV_B increase at the same rate. The difference between $\Delta\phi$ and ΔqV_B submonolayer coverages indicates that a positive dipole layer of magnitude 0.25 eV has formed. For a fractional surface coverage of ~4% measured by AES and XPS, this corresponds to a dipole moment of ~1.6 Debye or ~0.35 electrons Å/atom. Both Au on $(11\bar{2}0)$ CdSe and $(11\bar{2}0)$ intrinsic CdS produce comparable dipole layers of 0.3 eV.

The effect of Ag deposition on the surface work function and band bending of $(10\bar{1}0)$ CdS is shown in Fig. 12. The band bending decreases gradually to zero while the work function increases to a maximum at roughly 1 monolayer, then decreases

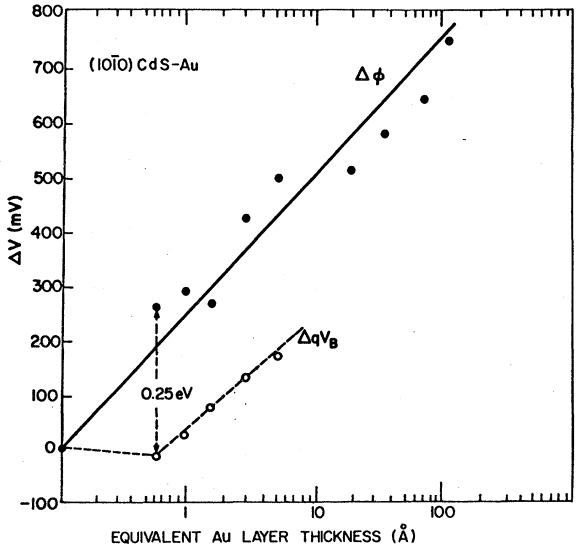

FIG. 11. Change in surface work function $\Delta\phi$ and band bending ΔqV_B plotted vs increasing metal overlayer thickness for Au on $(10\bar{1}0)$ CdS.

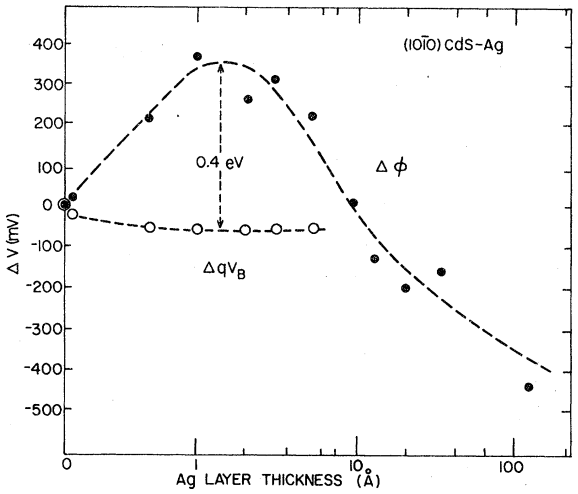

FIG. 12. Change in surface work function $\Delta\phi$ and band bending ΔqV_B plotted vs increasing metal overlayer thickness for Ag on (10$\bar{1}$0) CdS.

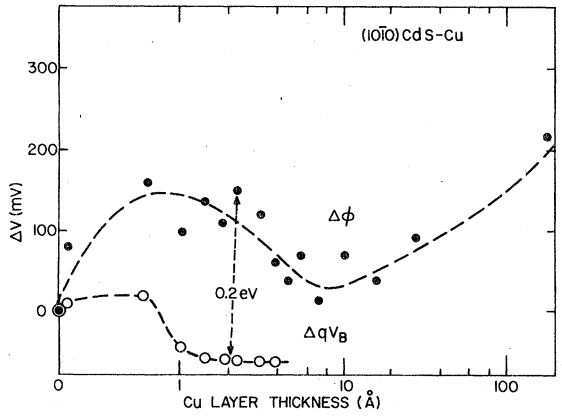

FIG. 13. Change in surface work function $\Delta\phi$ and band bending ΔqV_B plotted vs increasing metal overlayer thickness for Cu on (10$\bar{1}$0) CdS.

toward the work function of bulk Ag. This variation is significant because it accounts for the n-type band bending observed at Ag-CdS junctions,[41] despite the fact that the Ag work function is less than the electron affinity of CdS. This point is taken up in later sections.

Evaporation of Cu onto (10$\bar{1}$0) CdS also produces an effective increase in electron affinity as shown in Fig. 13. The work function also reaches a maximum at approximately one monolayer, then decreases. The subsequent increase in ϕ may be due to S diffusion and the formation of Cu_2S.[43] As in the case of Ag, the peak in ϕ at monolayer coverages accounts for the n-type band bending of Cu-CdS contacts even though the bulk Cu work function is less than the electron affinity of CdS. The magnitude of dipole formation also accounts for the ultimate Fermi-level position of the metal-semiconductor contact. Table II exhibits a comparison between the macroscopic Fermi-level position determined from internal photoemission measurements of barrier height[41] and the microscopic Fermi-level position determined from the maximum increase in surface-work function. The latter energy-level position is calculated from

$$E - E_v = E_g - (E_c - E_F) - \Delta\phi_{\max}, \qquad (2)$$

where $E_g = 2.5$ and 1.7 eV are the band gaps of CdS and CdSe, respectively, and $E - E_F = 0.1$ eV is the bulk Fermi-level position of each n-type semiconductor with respect to its conduction-band edge. The parameter $\Delta\phi_{\max}$ is the maximum change in surface work function due to dipole formation and band bending. For Au on CdS, the band bending and Fermi level continue to change after the initial dipole formation. For the other interfaces, the Fermi level stabilizes with the first few monolayers of metal coverage. Table II shows that the dipole-induced work function changes yield Fermi-level positions to within ~0.1 eV.

D. Fermi-level behavior of microscopic interface

Another gauge of local charge redistribution at these metal-semiconductor contacts is the com-

TABLE II. Comparison of Fermi level positions of macroscopic and microscopic metal-semiconductor interfaces. Barrier heights were determined from internal photoemission measurements of Mead (14). The maximum change in surface work function $\Delta\phi_{\max}$ due to dipole formation and band bending was measured by SPS.

Interface	Barrier height (eV)	Interface Fermi level above E_v (eV)	Metal-induced $\Delta\phi_{\max}$ (eV)	Contact Fermi level above E_v (eV)
Au-CdS	0.78	1.72	0.75	1.65
Ag-CdS	0.56	1.94	0.35	2.05
Cu-CdS	0.36	2.14	0.15	2.25
Au-CdSe	0.49	1.21	0.30	1.30

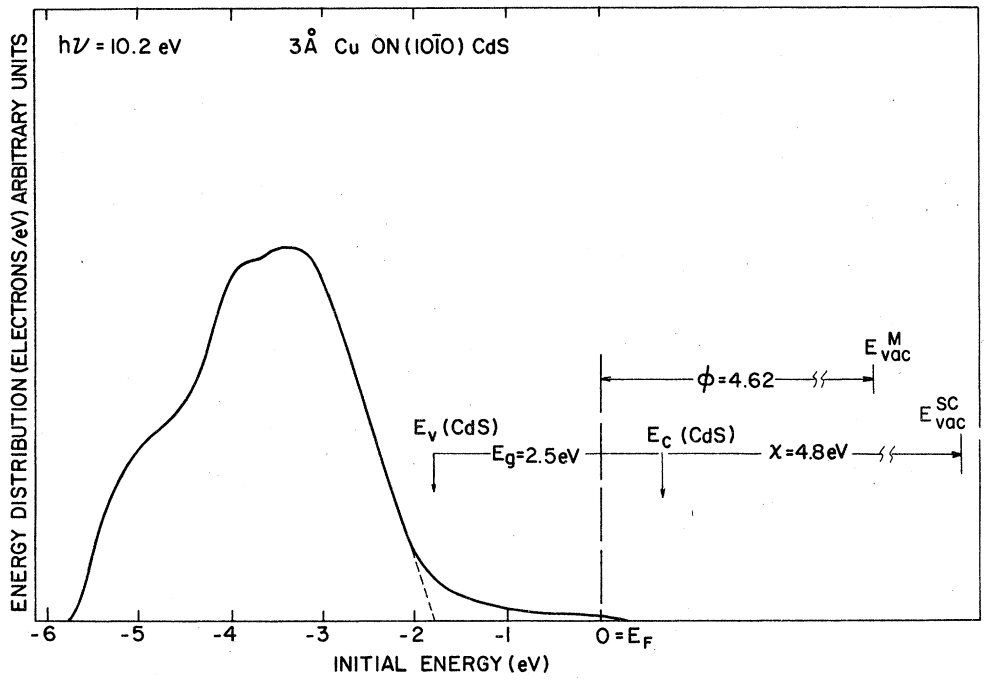

FIG. 14. Photoelectron spectra for a 3-Å Cu overlayer on cleaved (10$\bar{1}$0) CdS. The valence-band edge E_v and conduction-band edge E_c of CdS are determined relative to the extrapolated leading edge (dashed line) of the bulk CdS peak feature.

parison of surface work function and Fermi-level position as measured by UPS. The Fermi-level position relative to the semiconductor band edges was obtained from composite energy distribution curves (EDC's) of thin metal overlayers and semiconductor-substrates. Figure 14 illustrates such a composite UPS spectrum for 3 Å Cu on (10$\bar{1}$0) CdS. The cleaved CdS surface yields a character-

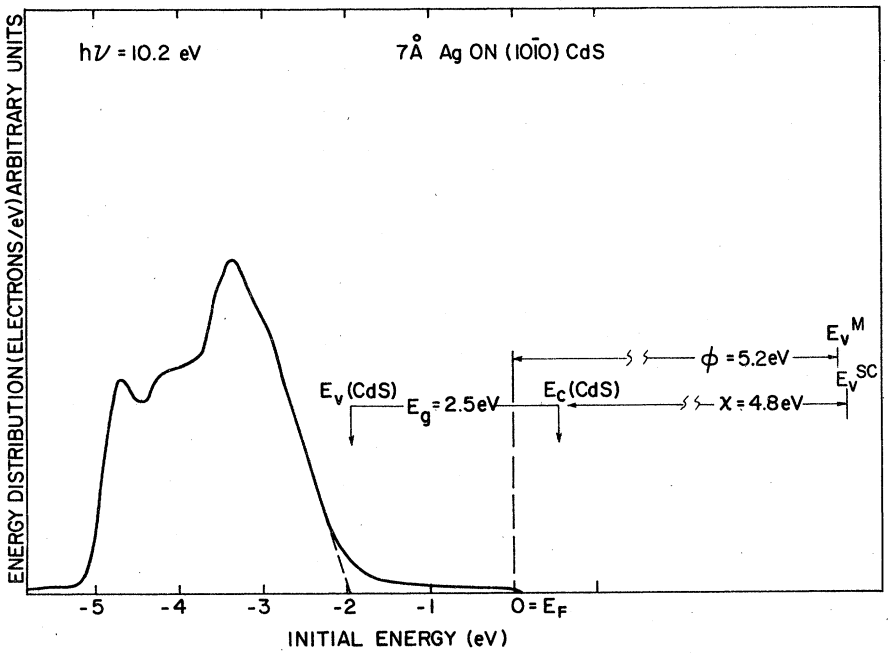

FIG. 15. Photoelectron spectra for a 7-Å Ag overlayer on cleaved (1010) CdS. The valence-band edge E_v and conduction-band edge E_c of CdS are determined relative to the extrapolated leading edge (dashed line) of the bulk CdS peak feature.

istic EDC which is easily separable from the composite metal-over-semiconductor spectra. This bulk CdS structure comprises the peak feature between −6 and −2 eV in Fig. 14 and is used to determine the valence-band edge E_v of CdS in the composite spectrum. The conduction-band edge E_c is then located from the energy gap value of 2.5 eV.[44] The EDC width of cleaved CdS yields an ionization energy of 7.3 eV, in agreement with results of Shay and Spicer[45] and thereby a CdS electron affinity of 4.8 eV. This last result confirms the absence of any surface contamination since CdS exposed to poorer vacuum conditions exhibits lower electron-affinity values.[45]

For 3 Å of Cu on CdS, an additional tail of states appears which defines the Fermi level in the band gap as shown. Photoemission from a thick Cu overlayer confirm that this energy is indeed the ultimate Fermi-level position. Figure 14 shows that a dipole layer must be formed since the work function of this surface $\phi = 4.62$ eV is less than the electron affinity $\chi = 4.8$ eV of CdS. This is indicated in Fig. 14 by the mismatch of metal and semiconductor vacuum levels $E^M_{\rm vac}$ and $E^{\rm SC}_{\rm vac}$, respectively.

Figure 15 shows a similar composite photoelectron spectrum for 7-Å Ag on CdS. Again, the tail of states above the leading edge of CdS structure defines the Fermi level in the band gap. The vacuum level mismatch $E^M_{\rm vac} - E^{\rm SC}_{\rm vac}$ indicates a dipole consistent with the work function variation in Fig. 12.

The Fermi-level positions of Ag and Cu on CdS measured by UPS are 2.05 ± 0.1 eV and 2.1 ± 0.1 eV above E_v, respectively, in good agreement with their ultimate Fermi-level positions as given in Table II. These positions do not shift appreciably with further metal coverage. Thus the ultimate Fermi-level positions of these metal semiconductor contacts are defined within the first one or two overlayers of metal coverage.

IV. DISCUSSION

Despite their reported difference in Schottky-barrier behavior with metals,[41] CdS and CdSe exhibit similar interface electronic features. Both CdS and CdSe show extrinsic electronic features due to interface chemical reactions, metal-induced surface states, and microscopic dipole formation. Furthermore, neither semiconductor has intrinsic surface states which can account for the interface band bending.

The qualitative difference between ELS measurements of reactive vs. unreactive metal-CdS and -CdSe interfaces leads to an estimate of the critical heat of interface reaction. Table III lists heats of interface reaction ΔH_R for common metals with CdS and CdSe. These ΔH_R values represent the most stable products of the reactions

$$M + (1/X)\mathrm{CdS} \rightarrow (1/X)(M_X\mathrm{S} + \mathrm{Cd}), \tag{3a}$$

$$M + (1/X)\mathrm{CdSe} \rightarrow (1/X)(M_X\mathrm{Se} + \mathrm{Cd}), \tag{3b}$$

where M is a metal atom, X is a coefficient, and ΔH_R is calculated per metal atom. Table III is divided into unreactive and reactive metal-semiconductor interfaces separated by an intermediate region. Stars mark compounds of the four metals studied by ELS. As shown, unreactive metals such as Au and Ag lie above the intermediate region while reactive metals such as Cu and Al are below it, so that the critical heat ΔH^C_R is ~0.5 eV/metal atom. This critical heat of reaction is greater than zero, reflecting the reduced energy needed to break semiconductor bonds in the surface and establish new bonds with the metal adsorbate. Reaction between a metal and a free semiconductor molecule would require more energy to completely dissociate the cation constituent of the semiconductor.

The divisions in Table III show that most metals react with CdS and CdSe surfaces. Furthermore the critical heat of reaction $\Delta H^C_R \sim 0.5$ eV/metal atom should apply at least as well to covalent semiconductors since their heats of formation are lower than those of CdS and CdSe (see Fig. 1), and interface compound formation is thus more likely. Andrews and Phillips have already shown a correlation between interface chemical reactivity and barrier heights for transition metals on Si,[46,47] and Bené and Walser have described this correlation in terms of a thin interface layer between metal and semiconductor.[48] Rowe *et al.*[2] have also attributed their ELS results for metals on Si to an intermediate region rather than a sharp interface boundary. Clearly the formation of interface compounds for metals on these semiconductors shows that intrinsic surface states, even if observed on the unperturbed semiconductor surface, are not relevant to the interpretation of Schottky-barrier behavior.

Heats of reaction ΔH_R also provide a more significant ordering of interface behavior than metal electronegativity. Despite the relationship between ΔH_F and ΔX,[19,20] metals with the same electronegativity, such as Ag and Cu, can exhibit qualtitatively different interface chemical behavior in contact with the same semiconductor. In addition, heats of reaction ΔH_R can be correlated with individual metal-semiconductor Schottky-barrier heights to reveal a transition in junction behavior between reactive and unreactive interfaces.[49]

The determination of interface reactivities by

TABLE III. Heats of reaction for common metals with CdS and CdSe ΔH values are for most stable compounds and are normalized per metal atom. Stars designate possible compounds of interfaces studied by ELS. The transition between reactive and unreactive metals indicates a critical heat of reaction $\Delta H_R^C \sim 0.5$ metal atom.

	Metal sulfide	Heat of reaction (eV/metal atom)		Metal selenide	Heat of reaction (eV/metal atom)
Unreactive	*AuS	3.94		*AuSe	1.36
	Bi_2S_3	1.99		HgSe	1.05
	HgS	1.00		WSe_2	1.05
				$FeS_{0.96}$	0.75
				$PtSe_{0.8}$	0.69
	PtS	0.69		SnSe	0.58
	*Ag_2S	0.61		*Ag_2Se	0.52
	PbS	0.53	ΔH_R^C	PbSe	0.46
	FeS	0.51		Bi_2Se	0.42
Reactive	*Cu_2S	0.50		*Cu_2Se	0.41
	SnS	0.43		In_2Se	0.16
	WS_2	0.41			
	$NiS_{0.67}$	0.29			
	InS	0.16			
	CrS	0.15			
	TaS_2	−0.57		MnSe	−0.10
	ZnS	−0.58		ZnSe	−0.15
	GaS	−0.62		Ga_2Se	−0.20
	MnS	−0.66		*Al_2Se_3	−0.69
	Cs_2S	−1.00			
	Ti_2S	−1.27		$TiSe_{1.5}$	−1.00
	*Al_2S_3	−1.43		MgSe	−1.54
	MgS	−2.10		$ThSe_{1.7}$	−2.66
	$ThS_{1.7}$	−3.53			

Eq. (3) and heats of formation does not take into account the microscopic kinetics of the adsorbed metal-semiconductor interface. In principle, the surface kinetics can be important in describing the course of interface reaction. However, they are apparently unnecessary for the description of the systems observed here since the interfaces reach equilibrium and no time-dependent phenomena are noticed. Furthermore, any analysis of the surface energetics is complicated by potential barriers due to charge and/or atomic rearrangement. To describe such processes from a kinetic point of view, one requires detailed information about the interface atomic positions.

The dipole formation observed for both reactive and unreactive interfaces dominates the Fermi-level movements which take place at the semiconductor surface during Schottky-barrier formation. These dipoles are in fact necessary to account for the n-type band bending which is produced on CdS and CdSe for metals with work functions ϕ_M less than the semiconductor electron affinities χ_{SC}. This situation is illustrated by the schematic energy-band diagram in Fig. 16(a). From UPS measurements here and elsewhere[45,50] $\chi_{CdS} = 4.8$ eV and $\chi_{CdSe} = 4.9$ eV. These are greater than the Cu and Ag work functions $\phi_{Cu} = 4.5$,[51] and $\phi_{Ag} = 4.0$,[52] respectively. According to a simple picture of interface charge transfer,[53] electrons should transfer from the metal into the semiconductor, causing the surface Fermi level E_F to rise with respect to the conduction-band edge E_c and thereby producing downward (p-type) band bending in the surface space-charge region. However, internal photoemission measurements of the surface barrier ϕ_B for Cu and Ag on CdS and CdSe show that the Fermi level actually moves to lower energies below E_c and that the bands bend upward.[41] Figures 12 and 13 show that this Fermi-level movement takes place within the first few monolayers of metal coverage and that the work function of the metal overlayer gradually decreases toward the bulk metal work function ϕ_M. Figure 16(b) illustrates a model for the spatial variation in energy bands which agree with the work function and Fermi-level measurements. As shown, a negative dipole layer forms at the intimate metal-semiconductor interface and the resultant discontinuity in local work function is screened out with distance into the metal. Although positive dipoles

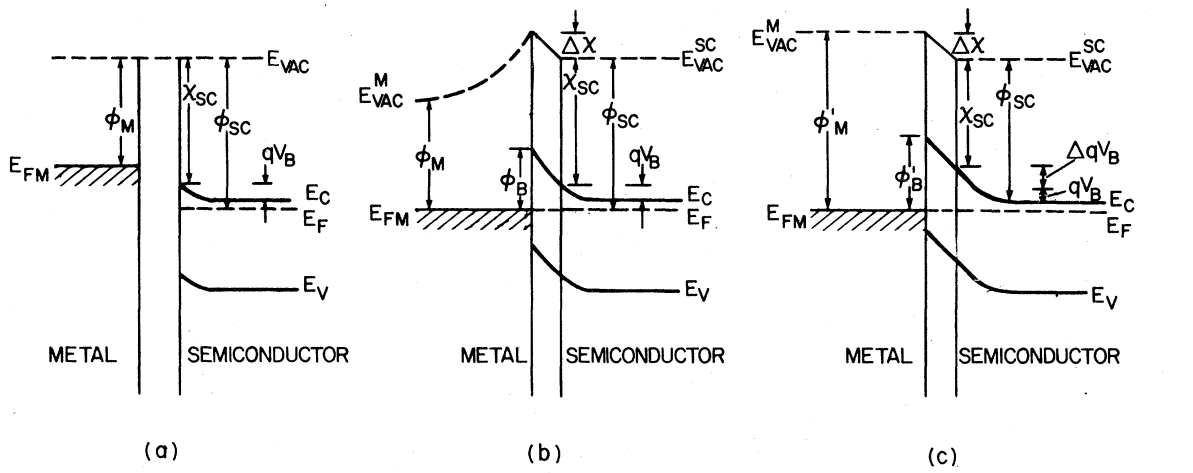

FIG. 16. Schematic energy band diagram of metal and semiconductor surface space charge region (a) at infinite separation, (b) after contact with no additional band bending, and (c) after contact with additional band bending. The interface region between metal and semiconductor is illustrated proportionally larger to display dipole effects.

are expected for the electron-donating metals, the negative dipoles observed may be due to metal-atom diffusion into the outermost plane of semiconductor atoms. Interdiffusion of metal and semiconductor atoms over thicknesses of several monolayers has already been observed for Au on III–V compound semiconductors[54] and Al on GaAs.[55] In the case where the band bending continues to increase with metal coverage, such as for Au on CdS, the variation in metal work function is minimal and the n-type band bending increases. As shown in Fig. 16(c), both the dipole energy $\Delta\chi$ and the change in band bending ΔqV_B can then contribute to the surface barrier ϕ'_B. In both cases, however, an interface dipole is required to account for the ultimate Fermi-level position of the contact.

The observation of dipole formation reported here is not unique to CdS and CdSe. Based on available electron affinity and work function values, some form of local charge redistribution is necessary to account for the sign and magnitude of barrier formation[14] for most metal-semiconductor contacts. Recent evidence for microscopic dipole formation in other semiconductor systems include measurements of Al, In, and Ga on Si,[1] Cs on InP,[11] Cs on GaSb,[8] and Cs on GaAs.[10] In each case, substantial changes in surface work function and electron affinity occur for monolayer or submonolayer metal coverages. Analogous to metals on CdS and CdSe, Cs on GaSb exhibits dipole formation in the absence of any intrinsic surface states.[8]

The interface dipole measurements reported here yield qualitative confirmation of the interface charge redistributions predicted by several theoretical calculations. Heine described charge tunneling from metal into semiconductor band gap to form short-range dipoles.[56] Pellegrini has recently treated the interface tunneling process in greater detail.[57] This phenomenon has been observed experimentally[58] and interpreted[59] for bulk metal-semiconductor junctions. The SPS results in this paper demonstrate that such charge redistribution takes place even before the metal atoms form a bulk Fermi level.

Louie and co-workers[60,61] have performed self-consistent pseudopotential calculations for microscopic metal-semiconductor interfaces which take into account the charge redistribution of the continuum states[62] as well as the band-gap electronic structure. As with the tunneling calculations, these results show that the influence of the metal overlayer extends only two or three layers into the semiconductor and that the outermost semiconductor atoms have slightly more negative charge than corresponding atoms deeper in the bulk. Self-consistent calculations of Applebaum and Hamann[63] also describe a highly localized dipole with the same sign.

The optical measurements of the intimate metal-CdS and -CdSe interfaces display no evidence for band-gap "closure" as predicted by the microscopic polarizability approach of Inkson.[64] On the other hand, the importance of interface chemical reactions in determining the electronic properties of these contacts is consistent with the chemical bonding approach of Andrews and Phillips,[46,47] which was used to correlate barrier heights with Si–transition-metal reactivity.

The spatial variation of the chemical and electronic data show that a microscopic theory of metal-semiconductor interfaces is required to describe the Schottky-barrier formation. Such a theory requires detailed information about the atomic positions of metal and semiconductor atoms. In general, this determination is complicated by reconstruction of the semiconductor surface, interdiffusion of metal and semiconductor atoms, and the formation of more than one surface bonding configuration. Characterization of surface molecular compounds via surface-sensitive UPS may provide a description of such interfaces.

V. CONCLUSIONS

Measurements of the surface electronic structure of CdS and CdSe during the initial stages of Schottky-barrier formation show that interface chemical reaction and local charge rearrangement rather than any intrinsic surface states of the semiconductor dominate the barrier-height properties. Despite their apparent difference in interface behavior, metals form dipoles on both CdS and CdSe. Both reactive and unreactive metals cause microscopic charge rearrangement and the local metal-semiconductor bonding of the first one or two monolayers control the ultimate Fermi level and barrier height of each junction.

ACKNOWLEDGMENTS

The author thanks Dr. R. Kellerman, Dr. C. B. Duke and Professor J. Bardeen for stimulating discussions.

[1]G. Margaritondo, J. E. Rowe, and S. B. Christman, Phys. Rev. B 14, 5396 (1976).
[2]J. E. Rowe, G. Margaritondo, and S. B. Christman, Phys. Rev. B 15, 2195 (1977).
[3]J. E. Rowe, S. B. Christman, and G. Margaritondo, Phys. Rev. Lett. 35, 1471 (1975).
[4]G. Margaritondo, S. B. Christman, and J. E. Rowe, J. Vac. Sci. Technol. 13, 329 (1976).
[5]Y. W. Chung, W. Siekhaus, and G. Somorjai, Phys. Rev. B 15, 959 (1977).
[6]P. E. Gregory and W. E. Spicer, Phys. Rev. B 6, 2370 (1975); W. E. Spicer, P. W. Chye, P. E. Gregory, T. Sukegawa, and I. A. Babalola, J. Vac. Sci. Technol. 13, 233 (1976).
[7]D. E. Eastman and J. L. Freeouf, Phys. Rev. Lett. 34, 1624 (1975).
[8]P. W. Chye, I. A. Babalola, T. Sukegawa, and W. E. Spicer, Phys. Rev. Lett. 35, 1602 (1975).
[9]P. W. Chye, T. Sukegawa, I. A. Babalola, H. Sunami, P. Gregory, and W. E. Spicer, Phys. Rev. B 15, 2118 (1977).
[10]W. E. Spicer, P. E. Gregory, P. W. Chye, I. A. Babalola, and T. Sukegawa, Appl. Phys. Lett. 27, 617 (1975).
[11]P. W. Chye, I. A. Babalola, T. Sukegawa, and W. E. Spicer, Phys. Rev. B 13, 4439 (1976).
[12]L. J. Brillson, *Proceedings of the* XIII *International Conference on Physics of Semiconductors*, edited by F. G. Fumi (Typografica Marves, Rome, 1976), p. 665.
[13]L. J. Brillson, Phys. Rev. Lett. 38, 245 (1977).
[14]C. A. Mead, Solid State Electron. 9, 1023 (1966), and references therein.
[15]J. Bardeen, Phys. Rev. 71, 717 (1947).
[16]S. Kurtin, T. C. McGill, and C. A. Mead, Phys. Rev. Lett. 22, 1433 (1970).
[17]C. A. Mead and T. C. McGill, Phys. Lett. A 58, 249 (1976).
[18]D. D. Wagman, W. H. Evans, V. B. Parker, I. Halow, S. M. Bailey, and R. H. Schumm, Natl. Bur. Stand. Technical Notes 270-3 (1968) and 270-4 (1969): Selected Values of Thermodynamic Properties (unpublished).
[19]J. C. Phillips and J. A. VanVechten, Phys. Rev. B 2, 2147 (1970).
[20]L. Pauling, *The Nature of the Chemical Bond*, 3rd ed. (Cornell Univ. Press, Ithaca, 1961).
[21]J. C. Tracy, in *Electron Emission Spectroscopy*, edited by W. Dekeyser, L. Fiermans, G. Vanderkelen, and J. Vennik (Reidel, Dordrecht, 1973), p. 295.
[22]I. Lindau and W. Spicer, J. Electron Spectrosc. 3, 409 (1974).
[23]L. J. Brillson, J. Vac. Sci. Technol. 12, 249 (1975).
[24]H. C. Gatos and J. Lagowski, J. Vac. Sci. Technol. 10, 130 (1973).
[25]L. J. Brillson, Surf. Sci. 51, 45 (1975).
[26]L. J. Brillson, Surf. Sci. 69, 62 (1977).
[27]L. J. Brillson, J. Vac. Sci. Technol. 13, 325 (1976).
[28]W. A. Coghlan and R. E. Clausing, At. Data 5, 317 (1973).
[29]P. W. Palmberg, G. E. Riach, R. E. Weber, and N. C. MacDonald, *Handbook of Auger Electron Spectroscopy* (Physical Electronics Ind., Edina, Minn., 1972).
[30]M. Creuzburg, Z. Phys. 196, 433 (1966).
[31]J. Daniels, C. v. Festenberg, H. Raether, and K. Zeppenfeld, Springer Tracts Mod. Phys. 54, 77 (1970), and references therein.
[32]J. L. Robins, Proc. Phys. Soc. Lond. 78, 1177 (1961).
[33]J. H. Scofield, J. Electron Spectrosc. 8, 129 (1976).
[34]L. J. Brillson and G. P. Ceasar, Surf. Sci. 58, 457 (1976).
[35]K. L. Chopra, *Thin Film Phenomena* (McGraw-Hill, New York, 1969), p. 166.
[36]J. L. Sullivan, J. Phys. D 6, 552 (1973).
[37]J. L. Sullivan, Thin Solid Films 25, 245 (1975).
[38]H. Raether, Springer Tracts Mod. Phys. 38, 84 (1965).
[39]J. Lagowski, C. L. Balestra, and H. C. Gatos, Surf. Sci. 29, 213 (1972).
[40]R. E. Halsted, M. Aven, and H. D. Coghill, J. Electrochem. Soc. 112, 177 (1965).
[41]C. A. Mead and W. G. Spitzer, Phys. Rev. 134, A713 (1964).
[42]S. G. Davisson and J. D. Levine, Solid State Phys. 25, 2 (1970), and references therein.
[43]L. R. Shiozawa, F. Austine, G. A. Sullivan, J. M. Smith, and W. R. Cook, Aeroscope Research Laboratories Report ARL 69-0155, 1969 (unpublished).

[44]R. H. Bube, Phys. Rev. 98, 431 (1955).
[45]J. L. Shay and W. E. Spicer, Phys. Rev. 169, 650 (1968).
[46]J. M. Andrews and J. C. Phillips, Phys. Rev. Lett. 35, 56 (1975).
[47]J. M. Andrews and J. C. Phillips, Crit. Rev. Solid State Sci. 5, 405 (1975).
[48]R. W. Bené and R. M. Walser, J. Vac. Sci. Technol. 14, 925 (1977).
[49]L. J. Brillson, Phys. Rev. Lett. 40, 260 (1978).
[50]R. K. Swank, Phys. Rev. 153, 844 (1967).
[51]W. F. Krolikowski and W. E. Spicer, Phys. Rev. 158, 514 (1967).
[52]D. E. Eastman, in *Techniques of Metal Research*, VI, edited by E. Passaglia (Interscience, New York, 1972), p. 411.
[53]See, for example, J. P. McKelvey, *Solid State and Semiconductor Physics* (Harper and Row, New York, 1966), p. 480.
[54]I. Lindau *et al.*, J. Vac. Sci Technol. March/April (1978).
[55]L. J. Brillson, J. Vac. Sci. Technol., March/April (1978).
[56]V. Heine, Phys. Rev. 138, A1689 (1963).
[57]B. Pellegrini, Phys. Rev. B 7, 5299 (1973).
[58]F. Steinrisser, L. C. Davis, and C. B. Duke, Phys. Rev. 176, 912 (1968).
[59]L. C. Davis and C. B. Duke, Phys. Rev. 184, 764 (1969).
[60]S. G. Louie, J. R. Chelikowsky, and M. L. Cohen, Phys. Rev. B 15, 2154 (1977).
[61]S. G. Louie, J. R. Chelikowsky, and M. L. Cohen, J. Vac. Sci. Technol. 13, 790 (1976).
[62]A. J. Bennett and C. B. Duke, Phys. Rev. 162, 578 (1967); and C. B. Duke, J. Vac. Sci. Technol. 6, 152 (1969).
[63]J. A. Appelbaum and D. R. Hamann, *Proceedings of the* XII *International Conference on Physics of Semiconductors*, edited by M. H. Pilkuhn (Teubner, Stuttgart, 1976), p. 675.
[64]J. C. Inkson, J. Phys. C 6, 1350 (1973).